ARTICLES

Unipolar-to-Ambipolar Conversion of Organic Thin-Film Transistors by Organosilane Self-Assembled Monolayer

Jung Hwa Seo,[†,‡] Gap Soo Chang,[*,§] Regan G. Wilks,[§] Chung Nam Whang,[*,†] Keun Hwa Chae,[∥] Seongjin Cho,[⊥] Kyung-Hwa Yoo,[†] and Alexander Moewes[§]

Institute of Physics and Applied Physics, Yonsei University, Seoul 120-749, Korea, Department of Physics and Engineering Physics, University of Saskatchewan, Saskatoon SK S7N 5E2, Canada, Division of Materials Science and Technology, Korea Institute of Science and Technology, Seoul 130-791, Korea, and Department of Physics, Kyungsung University, Busan, 608-736, Korea

Received: August 17, 2008; Revised Manuscript Received: October 18, 2008

Simplification of the design and manufacture of electronic and optoelectronic devices, such as field-effect transistors and light emitting diodes, can be achieved with the use of organic semiconductor materials. Organic thin-film field-effect transistors (TFFETs) can be used to complement current metal-oxide semiconductor technology, provided that organic ambipolar transistors can be configured to operate in both p-channel and n-channel configurations. The development of organic ambipolar TFFETs has been hindered by the lack of n-type conduction in most of the common organic TFFETs. Here, we show that we can achieve high ambipolar carrier mobility in TFFETs based on rubrene and pentacene molecules through the inclusion of an organosilane self-assembled monolayer (SAM) on the gate dielectric surface. A similar device that lacks the aforementioned SAM exhibits only p-type characteristics, confirming that the enhancement of the n-type conductivity is due to the passivation of the dielectric surface that results from the inclusion of organosilane monolayer.

Organic semiconductors are intrinsically capable of transporting both p-type (holes) and n-type (electrons) carriers, although many organic-based thin-film field-effect transistors (TFFETs) exhibit unipolar (predominantly p-type) field-effect conduction.[1−4] Inhibition of the carrier injection from metal electrodes to the organic semiconductors has been implicated in the suppression of n-type conductivity.[1,5] The carrier injection barrier is related to the position of the metal electrode's work function relative to the highest occupied and lowest unoccupied molecular orbitals (HOMO and LUMO, respectively) of the organic materials. However, merely reducing the barrier through the use of a low-work-function electrode does not correct the problem; the TFFETs produced in this way still exhibit unipolar, or p-type dominant, conduction.[3,6,7] The use of a hydroxyl-free gate dielectric has meanwhile been shown to promote n-channel transistor operation in a variety of conjugated polymers, indicating that the interface between the organic semiconductor material and the gate dielectric has a significant effect on the carrier transport.[3,8] This finding suggests that ambipolar TFFETs may be developed by modifying the surface characteristics of the SiO_2 gate dielectric by including an organosilane self-assembled monolayer (SAM) prior to the deposition of organic active layers.

The two representative molecules with relatively high field-effect mobility, rubrene and pentacene, have been chosen for this study (see Figure 1a). Rubrene, consisting of a tetracene backbone and four phenyl side groups, has high field-effect mobility of 15 $cm^2\ V^{-1}\ s^{-1}$ when in crystalline form,[9,10] and it is therefore a very promising candidate for organic electronics applications. However, rubrene's nonplanar molecular geometry has made the fabrication of highly ordered rubrene crystalline thin film very difficult.[11,12] When a rubrene thin film is grown directly onto SiO_2 dielectric, an amorphous phase is formed and the resulting rubrene TFFET exhibits extremely low field-effect mobility in the range of $10^{-4}-10^{-6}$ $cm^2\ V^{-1}\ s^{-1}$.[13,14] To overcome this limitation, pentacene has been employed due to the formation of a low-energy interface with SiO_2.[15] Octadecyltrichlorosilane (OTS), consisting of a long-chain alkyl group ($C_{18}H_{37}$) and a polar headgroup ($SiCl_3$), has also been employed to passivate the surface of the SiO_2 gate dielectric before the deposition of organic semiconductors. In the present study, we demonstrate that when organic TFFETs with rubrene/pentacene heterostructure are fabricated on an OTS-SAM-treated SiO_2 gate dielectric, the passivation of electron carrier traps leads to high field-effect mobility for both holes and electrons.

A schematic of the device is shown in Figure 1b. We have fabricated bottom-gate TFFETs on a heavily doped silicon substrate with a 100 nm thick SiO_2 gate dielectric that was grown using a dry oxidation process. The OTS-SAM was formed by immersing the SiO_2/Si substrates in a 0.1 mM solution of OTS in hexane for 1 h. The substrates were then cleaned in hexane to remove the residual OTS, followed by

* To whom correspondence should be addressed. Phone: +1-306-966-2768 (G.S.C.); +82-2-2123-2613 (C.N.W.). Fax: +1-306-966-6400 (G.S.C.); +82-2-392-1592 (C.N.W.). E-mail: gapsoo.chang@usask.ca (G.S.C.); chwhang@yonsei.ac.kr (C.N.W.).

† Yonsei University.

‡ Current address: Center for Polymer and Organic Solids, Department of Chemistry and Biochemistry, University of California, Santa Barbara, CA.

§ University of Saskatchewan.

∥ Korea Institute of Science and Technology.

⊥ Kyungsung University.

10.1021/jp807355q CCC: $40.75
Published on Web 11/24/2008

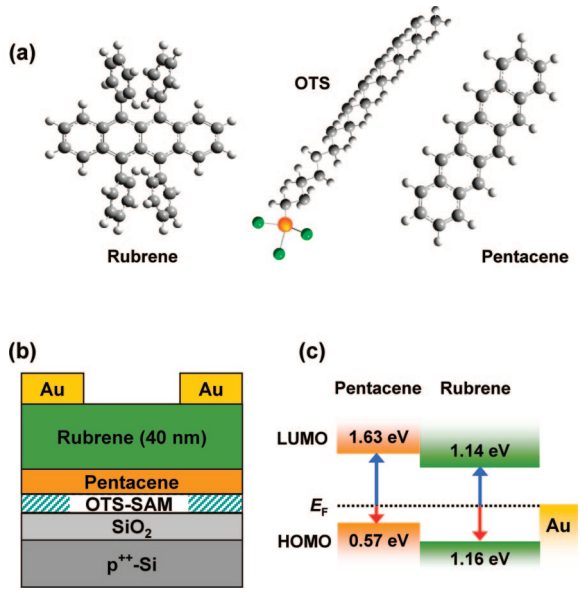

Figure 1. (a) Molecular structures of related organic molecules (rubrene, OTS, and pentacene). (b) Schematic illustration of ambipolar TFFETs with rubrene/pentacene on the OTS-SAM-treated SiO_2. (c) Energy-level alignment of rubrene and pentacene in contact with Au electrodes. The blue (red) arrows indicate the energy positions of LUMO (HOMO) levels for rubrene and pentacene with respect to the Fermi level of Au.

drying under blowing N_2 gas. The pentacene as the first organic active layer was deposited with controlling the thickness of 2 and 10 nm. Subsequently, 40 nm rubrene as the second organic active layer was deposited onto the pentacene layer. The base pressure was 1×10^{-8} Torr, and the deposition rate was maintained at 0.1 Å/s for both rubrene and pentacene. Finally, 35 nm thick Au source and drain electrodes were formed through a shadow mask by thermal evaporation to provide a channel length of 50 μm and a channel width of 1000 μm.

The electrical measurements of the device characteristics were performed using a Keithley 4200-SCS source-measurement unit at ambient pressure and room temperature. A negative (positive) gate bias was applied to operate the transistors in the hole (electron) accumulation mode. The structural and morphological properties were investigated using X-ray diffraction (XRD) and atomic force microscopy (AFM), respectively. The XRD measurements were carried out at beamline 10C1 of the Pohang Light Source at the Pohang Accelerator Laboratory. The wavelength of incident X-rays was 1.5425 Å. Due to the surface softness of organic films, tapping mode AFM images were obtained in air using a MultiMode microscope with a Nanoscope controller IIIa (Veeco). The occupied carbon 2p partial density of states was probed by employing resonant X-ray emission spectroscopy (RXES). The emission measurements were conducted at beamline 8.0.1 of the Advanced Light Source at the Lawrence Berkeley National Laboratory. The excitation energies for carbon Kα (2p $\rightarrow$ 1s transition) emission spectra were selected at the π^*-absorption threshold (285.4 eV).

Figure 1c depicts the energy levels of rubrene and pentacene aligned with respect to the Fermi level (E_F) of Au. When rubrene is deposited on pentacene, the HOMO level of rubrene is located at 1.16 eV with respect to the E_F value of the Au electrode, and the magnitude of the injection barrier for electrons (LUMO level) is similar (1.14 eV). This suggests that both hole and electron transport is probable in transistors with rubrene/pentacene structure, even though rubrene-based field-effect transistors (FETs) have been shown to be strong p-channel transistors.[9,16−18] Even using a rubrene single crystal, the electron field-effect mobility (μ_n) of rubrene FETs has been shown to be 2 orders of magnitude weaker than the hole mobility (μ_p).[19]

Figure 2 shows the output characteristics of the TFFETs with rubrene/pentacene heterostructure on the OTS-SAM-treated SiO_2 gate dielectric. One can clearly observe that these TFFETs operate in both the hole-accumulation (p-channel) and electron-accumulation (n-channel) modes, while the devices without OTS-SAM show characteristics of a unipolar transistor. In the p-channel operation, the plots of drain current (I_D) versus drain-source voltage (V_{DS}) at different gate voltages (V_G) show that the I_D grows linearly before saturating as the negative V_{DS} increases (top panels in Figure 2b and d). For low V_G and high V_{DS}, the I_D increases abruptly with increasing (negative) V_{DS}. This steep increase in I_D is typical of an ambipolar transistor due to the n-type conductivity at the drain electrode. In such a case, a source-drain bias much higher than V_G can induce an electron-accumulation region near the drain electrode as well as the normal hole-accumulation region at the source electrode. The hole-rich source and electron-rich drain form a pn junction, causing I_D flow even at low V_G.[20] The n-channel device operation also exhibits a similar increase of I_D due to the drain-induced holes at high V_{DS} and low V_G (bottom panels in Figure 2b and d). The I_D response for both transistors is nonlinear for low V_{DS} in the n-channel operation, indicating the presence of an energy barrier for electron transport. This barrier is presumably influenced by two interfacial factors: the electron injection from the high-work-function Au electrode (5.1 eV) into rubrene and the energy-level misalignment of the rubrene and pentacene (the LUMO of pentacene is 0.49 eV higher than that of rubrene, as shown in Figure 1c). By using a model equation for the saturation regime,[21] the μ_p and μ_n of OTS-SAM-treated transistors are derived from carrier-transfer characteristics presented in Figure 3. The transistor with rubrene on 2 nm pentacene has a μ_p value of 1.1×10^{-3} cm^2 V^{-1} s^{-1} (at $V_D = -60$ V) and a μ_n value of 0.07×10^{-3} cm^2 V^{-1} s^{-1} (at $V_D = 60$ V). The use of a thicker pentacene (10 nm) enhances the field-effect mobility of both carriers, and μ_n (0.05 cm^2 V^{-1} s^{-1}) becomes comparable to μ_p (0.08 cm^2 V^{-1} s^{-1}). This value of μ_n is the highest ever reported for a rubrene-based FET under ambient conditions. It should be noted that the ambipolar transport behavior is absent in the TFFETs fabricated without an OTS-SAM passivation of SiO_2 (see Figure 2a and c). Although the transistors without OTS-SAM are operable only in the p-channel mode, a similar enhancement of μ_p is observed when the pentacene thickness increases.

In order to better understand the electrical characteristics of our TFFETs, the crystallinity and morphology of rubrene surfaces onto pentacene with a thickness of 2 and 10 nm on top of OTS-SAM-treated SiO_2 are investigated by XRD and AFM. Parts a−d and e−h of Figure 4 show, respectively, the XRD patterns and AFM images of 40 nm rubrene thin films grown on various bottom-layer configurations. One can see that existence of a pentacene layer and treatment of OTS-SAM on SiO_2 play an important role in improving the crystallinity of the rubrene. The absence of diffraction features shows that a rubrene single layer deposited directly onto the OTS-SAM-treated SiO_2 is amorphous, and thus, the corresponding AFM image (Figure 4e) shows simple aggregation of randomly oriented rubrene molecules. On the other hand, two diffraction peaks around 6 and 20° appear in the rubrene film on a 2 nm pentacene layer, and multiple-diffraction features become apparent in the spectrum from the film with a 10 nm pentacene layer. The *d*-spacing of the rubrene film corresponding to (00*l*)

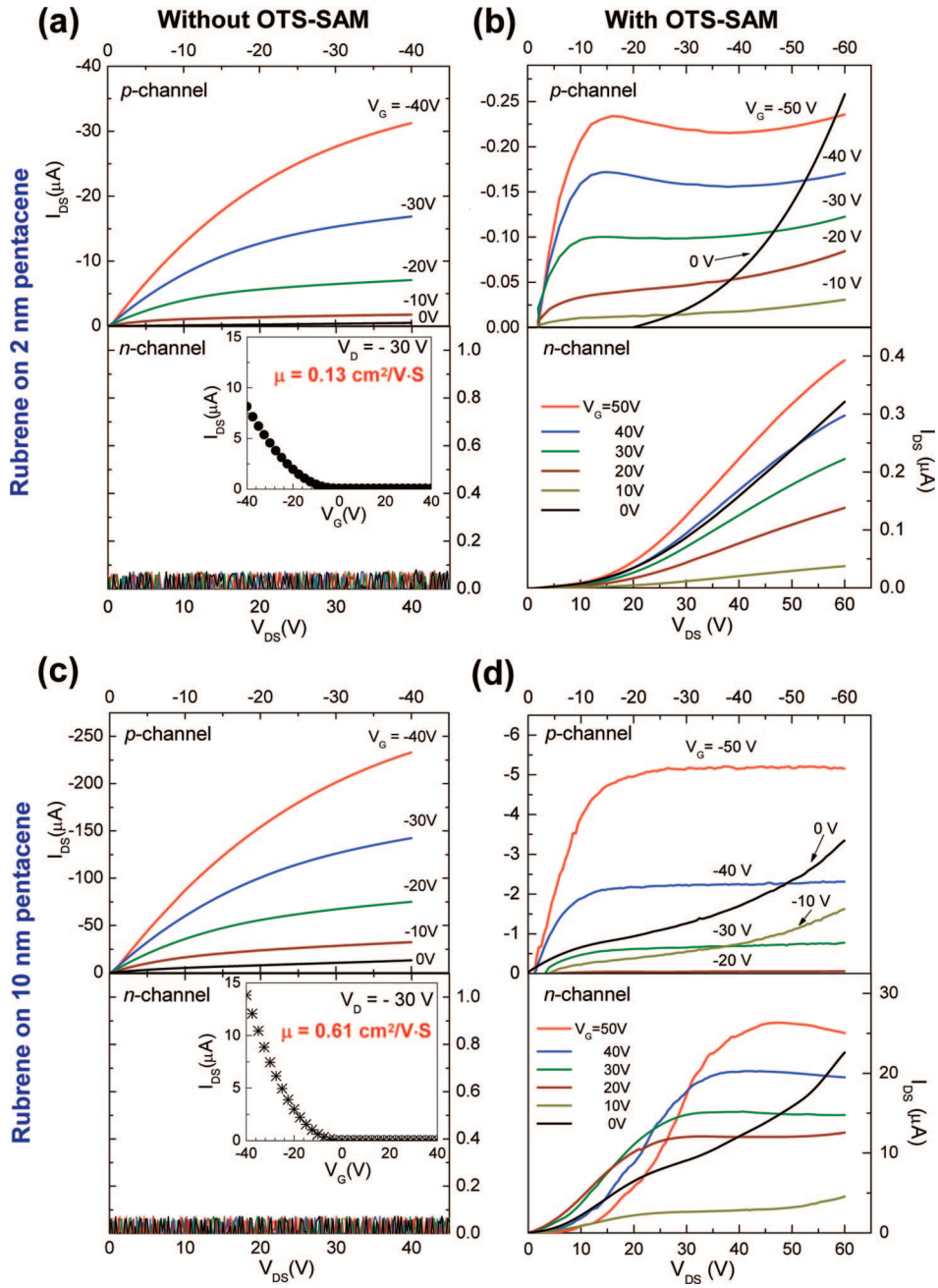

Figure 2. Output characteristics of the TFFETs fabricated with OTS-SAM. The TFFETs fabricated rubrene on (a) 2 nm and (c) 10 nm pentacene layers without OTS-SAM, and the devices fabricated rubrene on (b) 2 nm and (d) 10 nm pentacene with OTS-SAM (b, d) operating in hole-accumulation (top panels) and electron-accumulation (bottom panels) mode. The insets in the bottom panels of parts a and c represent the transport characteristics of corresponding samples operating in p-channel mode.

multiple-diffraction peaks at 6.51, 13.15, 19.75, and 26.44° is determined to be 13.5 Å, which confirms the orthorhombic rubrene structure and agrees well with the half-length of the *c*-axis lattice parameter (26.97 Å).[15,16] In addition, the (00*l*) diffraction peaks from the pentacene layer in Figure 4c indicate that a 10 nm pentacene layer has a highly ordered triclinic (P1 group) structure with a *d*-spacing of 15.71 Å. These XRD patterns are consistent with the morphological features of the corresponding samples. The use of a 2 nm pentacene layer stimulates the crystallization of rubrene molecules, but the rubrene upper layer is very porous and contains rod-shaped grains. This is reflected in the low field-effect mobility of our TFFETs with a thin pentacene layer; the porosity of the organic active layer in a transistor not only leads to poor contact with Au electrode but also inhibits intergranular carrier transport. If the pentacene layer is sufficiently thick and crystallized, however, a highly packed rubrene crystalline thin film can be obtained, as shown in Figure 4c and g. The high crystallinity of the rubrene thin film provides a smooth interface and low contact resistance, leading to an order of magnitude increase in the carrier mobility over the TFFETs fabricated with a 2 nm pentacene layer (Figure 3).

Although the structural and morphological results clearly reflect the enhancement of the field-effect mobility due to the insertion of the thicker pentacene layer, the induction of ambipolar conductivity in TFFETs cannot be solely explained by the presence of a pentacene layer. We note that the crystallization of rubrene molecules can be similarly improved without the OTS-SAM treatment (see Figure 4d and h). According to the energy-level diagram in Figure 1c, the HOMO

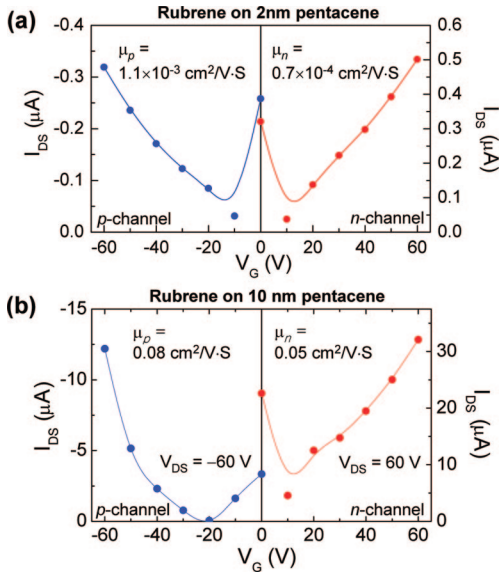

Figure 3. Transport characteristics of the ambipolar TFFET with rubrene on (a) 2 nm and (b) 10 nm of pentacene/OTS-SAM operating in hole-accumulation at $V_{DS} = -60$ V (blue lines) and electron-accumulation at $V_{DS} = 60$ V (red lines) mode.

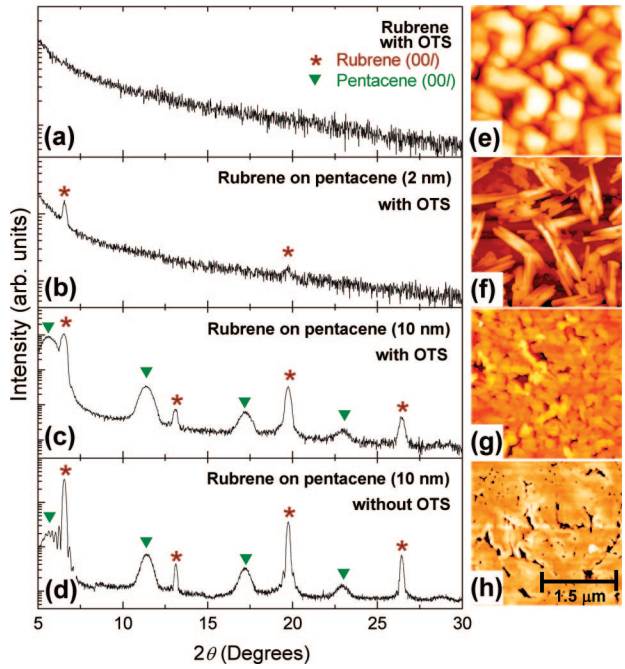

Figure 4. Structural and morphological properties of rubrene films on various bottom-layer configurations. XRD patterns of rubrene layers (a) on the OTS-SAM-treated SiO_2, (b) on 2 nm of pentacene/OTS-SAM, (c) on 10 nm of pentacene/OTS-SAM, and (d) on a 10 nm thick pentacene layer without the OTS-SAM. (e−h) AFM images of corresponding samples.

level of pentacene is aligned closer to the E_F value of Au than that of rubrene, resulting in an efficient injection of holes into the pentacene layer, and thus, pentacene provides an accumulation layer for holes which are effectively transported through a high-quality rubrene top layer. On the other hand, a low electron-injection barrier of rubrene with respect to pentacene can confine electrons at the rubrene/pentacene interface. This is in accordance with the nonlinear I_D response of TFFETs for low V_{DS} during the n-channel operation (Figure 2b and d). However, the devices fabricated without the OTS-SAM show no n-type conductivity regardless of the pentacene thickness, although

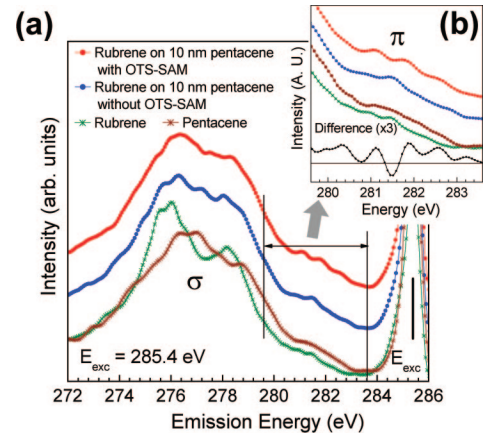

Figure 5. (a) Carbon Kα RXES spectra for TFFETs with a rubrene layer on the OTS-SAM-treated SiO_2 with no pentacene layer (green line), on 10 nm of pentacene/OTS-SAM (red line), and on 10 nm of pentacene without OTS-SAM (blue line). A reference spectrum of pentacene (brown line) is also included. The peaks on the right side of the spectra indicate the elastic peaks corresponding to the excitation energy (E_{exc}) of 285.4 eV. (b) The enlarged spectra in the π-state region. The black line indicates the spectral difference between TFFETs with (red) and without OTS-SAM (blue).

we have designed TFFETs with a stepwise barrier to make the electron transport easy. These provide direct evidence that the suppression of n-type conductivity in TFFETs without OTS-SAM is related to the character of the semiconductor/dielectric interface.

Recently, Chua et al. suggested that the n-type conduction in various conjugated polymers can be significantly influenced by the hydroxyl groups in an oxide dielectric, which act as strong electron traps.[3] In the SiO_2 dielectric, the hydroxyl groups are present in the form of SiOH silanols and have a tendency to self-stabilize by capturing electrons. The trapped electrons build a negative field at the semiconductor/dielectric interface and ultimately suppress the positive gate voltage required for the n-channel transistor operation. The inhibition of n-type conduction in TFFETs, which we have overcome with the OTS-SAM treatment, can be attributed to this electron trapping at the semiconductor/dielectric interface. In our TFFET structure, the LUMO of pentacene is higher than rubrene, but the barrier for electron transfer across the rubrene/pentacene interface is rather small. One can thus expect the electrons to easily reach the SiO_2 surface, as the V_G increases positively for the n-channel operation. Attaching an OTS molecule to the SiO_2 surface causes the SiOH silanols to be passivated into covalent siloxane (Si−O−Si) bonds. The passivation mechanism consists of a reaction of the silanol with the OTS polar headgroup ($-SiCl_3$), leading to a release of HCl, while the opposite end of the long-chain alkyl group ($-C_{18}H_{37}$) in OTS remains available for bonding to the organic active layer (pentacene, in our case), effectively eliminating electron trapping at the interface with the SiO_2 gate dielectric.[22]

The chemical reaction of organic layers with the OTS-SAM-treated SiO_2 was investigated using a RXES technique, a photon-in/photon-out process in RXES that can be used to determine chemical-selective information from a deeply buried interface. Figure 5 shows carbon Kα RXES spectra of ambipolar TFFETs with and without the OTS-SAM. The spectra reflect the carbon 2p density of occupied states; the incoming X-rays were tuned such that the excitation energy (E_{exc}) corresponded to the π^*-absorption threshold (285.4 eV). The spectra measured from the transistors with rubrene/pentacene heterostructure differ from

those of the device based on an amorphous rubrene single layer. These differences are expected, because the RXES spectra contain contributions from both rubrene and pentacene layers. Particularly, the valence center of π-states shifts toward higher emission energy (lower binding energy). The effect of the OTS-SAM treatment on the electronic structure of the active layers was examined by subtracting the spectrum of ambipolar TFFETs without OTS-SAM from that measured from the sample treated with OTS-SAM. The spectral difference in the π-states seen in Figure 5b clearly shows more density of π-states at high emission energy (low binding energy) in the spectrum measured from the OTS-SAM-containing sample, indicating that pentacene molecules are reacting with the alkyl group of OTS-SAM instead of the silanols in SiO_2. Therefore, the dielectricity of OTS can effectively prevent electrons from reaching the surface of SiO_2. These results suggest that depositing OTS-SAM onto the SiO_2 gate dielectric provides an effective way to avoid the problem of electron trapping. Clearly, the successful development of ambipolar TFFETs hinges on the ability to appropriately modify the surface of the SiO_2 gate dielectric prior to the addition of the organic active layer as well as the consideration of proper energy-level alignment.

We have demonstrated that high carrier mobility for both holes and electrons can be achieved in TFFETs that had previously shown a strong disposition toward p-type conductivity through passivation of the SiO_2 gate dielectric surface with an OTS-SAM. This treatment serves to minimize the charge trapping tendencies at the organic/dielectric interface, showing that the elimination of this effect is as important to the design of high-performance ambipolar TFFETs as is energy-level matching between the various layers. As a result of these findings, we expect an enhanced applicability of these devices in the development of organic-based complementary logic circuitry.

Acknowledgment. This work was supported by the Brain Korea 21 (BK21) project of Korea Research Foundation (KRF) and Korea Science and Engineering Foundation (KOSEF) through National Core Research Center for Nanomedical Technology. We gratefully acknowledge the Natural Sciences and Engineering Research Council of Canada and the Canada Research Chair program.

References and Notes

(1) Meijer, E. J.; Leeuw, D. M. De.; Setayesh, S.; Veenendaal, E. V.; Huisman, B.-H.; Blom, P. W. M.; Hummelen, J. C.; Scherf, U.; Klapwijk, T. M. *Nat. Mater.* **2003**, *2*, 678–682.

(2) Menard, E.; Podzorov, V.; Hur, S.-H.; Gaur, A.; Gershenson, M. E.; Rogers, J. A. *Adv. Mater.* **2004**, *16*, 2097–2101.

(3) Chua, L.-L.; Zaumseil, J.; Chang, J.-F.; Ou, Eric C.-W.; Ho, Peter K.-H.; Sirringhaus, H.; Friend, R. H. *Nature* **2005**, *434*, 194–199.

(4) Dimitrakopoulos, C. D.; Purushothaman, S.; Kymissis, J.; Callegari, A.; Shaw, J. M. *Science* **1999**, *283*, 822–824.

(5) Yan, X.; Wang, J.; Wang, H.; Wang, H.; Yan, D. *Appl. Phys. Lett.* **2006**, *89*, 053510.

(6) Yasuda, T.; Goto, T.; Fujita, K.; Tsutsui, T. *Appl. Phys. Lett.* **2004**, *85*, 2098–2100.

(7) Takenobu, T.; Takahashi, T.; Takeya, J.; Iwasa, Y. *Appl. Phys. Lett.* **2007**, *90*, 013507.

(8) Singh, Th. B.; Meghdadi, F.; Günes, S.; Marjanovic, N.; Horowitz, G.; Lang, P.; Bauer, S.; Sariciftci, N. S. *Adv. Mater.* **2005**, *17*, 2315–2320.

(9) Podzorov, V.; Menard, E.; Borissov, A.; Kiryukhin, V.; Rogers, J. A.; Gershenson, M. E. *Phys. Rev. Lett.* **2004**, *93*, 086602.

(10) Sundar, V. C.; Zaumseil, J.; Podzorov, V.; Menard, E.; Willett, R. L.; Someya, T.; Gershenson, M. E.; Rogers, J. A. *Science* **2004**, *303*, 1644–1646.

(11) Kowarik, S.; Gerlach, A.; Sellner, S.; Schreiber, F.; Pflaum, J.; Cavalcanti, L.; Konovalov, O. *Phys. Chem. Chem. Phys.* **2006**, *8*, 1834–1836.

(12) Käfer, D.; Ruppel, L.; Witte, G.; Wöll, Ch. *Phys. Rev. Lett.* **2005**, *95*, 166602.

(13) Seo, S.; Park, B.-N.; Evans, P. G. *Appl. Phys. Lett.* **2006**, *88*, 232114.

(14) Park, S.-W.; Hwang, J. M.; Choi, J.-M.; Hwang, D. K.; Oh, M. S.; Kim, J. H.; Im, S. *Appl. Phys. Lett.* **2007**, *90*, 153512.

(15) Seo, J. H.; Pedersen, T. M.; Chang, G. S.; Moewes, A.; Yoo, K.-H.; Cho, S. J.; Whang, C. N. *J. Phys. Chem. B* **2007**, *111*, 9513–9518.

(16) Fong, H. H.; So, S. K.; Sham, W. Y.; Lo, C. F.; Wu, Y. S.; Chen, C. H. *Chem. Phys.* **2004**, *298*, 119–123.

(17) Briseno, A. L.; Tseng, R. J.; Ling, M.-M.; Falcao, E. H. L.; Yang, Y.; Wudl, F.; Bao, Z. *Adv. Mater.* **2006**, *18*, 2320–2324.

(18) Goldmann, C.; Krellner, C.; Pernstich, K. P.; Haas, S.; Gundlach, D. J.; Batlogg, B. *J. Appl. Phys.* **2006**, *99*, 034507.

(19) Takahashi, T.; Takenobu, T.; Takeya, J.; Iwasa, Y. *Appl. Phys. Lett.* **2006**, *88*, 033505.

(20) Neudeck, G. W.; Bare, H. F.; Chung, K. Y. *IEEE Trans. Electron Devices* **1987**, *34*, 344–350.

(21) Horowitz, G. *Adv. Mater.* **1998**, *10*, 365–377.

(22) Barriga, J.; Coto, B.; Fernandez, B. *Tribol. Int.* **2007**, *40*, 960–966.

JP807355Q